Analysis and optimisation of a gas-cooled pipe for solar thermal energy production using parabolic collectors

C. Aragonese, S. Buono, L. Maciocco, V. Moreau, L. Sorrentino

CRS4, Centre for Advanced Studies, Research and Development in Sardinia

March 2000

Abstract

In the framework of the design of a solar thermal power plant proposed by ENEA, the activity carried out by CRS4 on the thermal-fluid-dynamic simulation of a gas-cooled pipe irradiated by a parabolic solar collector is described in this paper.

Two methods have been adopted in parallel: a simplified one-dimensional approach and a Computational-Fluid-Dynamics (CFD) three-dimensional approach. The first method was used to build a tool able to give quick answers to parameters changes with an acceptable degree of accuracy. The CFD analysis is used both to validate 1D-model results and to study in details all 3D physical phenomena.

The multi-zone one-dimensional model developed at CRS4 is described first. The pipe is split along its axis into a discrete number (typically 100) of sub-domains. Each sub-domain is split further on into five different zones, corresponding to the various components of the pipe. All the main energy-exchange mechanisms between the various parts of the pipe have been implemented, resulting in a system of five equations for each sub-domain, solved iteratively within an EXCEL framework.

The 3D-CFD model is then described. The model is fully parametric, allowing a quick variation of the geometrical parameters of the system. Convection, conduction and thermal radiation heat exchanges are solved in a coupled way. The model can give any information about field variables of fluids and solid structures as well as all energy balances.

The two models have been used for a parametric study of the effect of the pipe diameter variation on the system efficiency. Although not negligible differences between the two models can be noticed concerning local energy balances, the error on the evaluation of the system efficiency is order 1%. The result of the optimisation was practically the same for the two models.

Table of contents

1 Introduction

The Italian Agency for Energy and Environment (ENEA) is developing the design of the thermal solar plant proposed by C. Rubbia [1, [2], based on high-temperature linear-parabolic collectors.

The efficiency of the solar collection system is based on a balance between the following contributions:

collected solar radiation;

heat loss from the collector pipe to the environment;

pumping power.

The system efficiency depends on the geometry and disposition of the parabolic mirrors [1], on the geometrical characteristics of the collector pipe and on the radiating characteristics of the pipe surfaces.

CRS4 has the task of producing a computational model able to simulate with a high degree of accuracy the thermal-fluid-dynamics of the collector pipe and to optimise it on the basis of the specifications given by ENEA.

2 Overall description

The system consists of a 100 m long circular pipe irradiated by a linear parabolic solar collector.

The pipe (Figure 1) is made of steel or, optionally, by a double layer of steel and copper, in order to enhance thermal conduction. The pipe is insulated form external air by a glass pipe. Void is made in the space between the glass tube and the metal tube in order to inhibit convection heat losses.

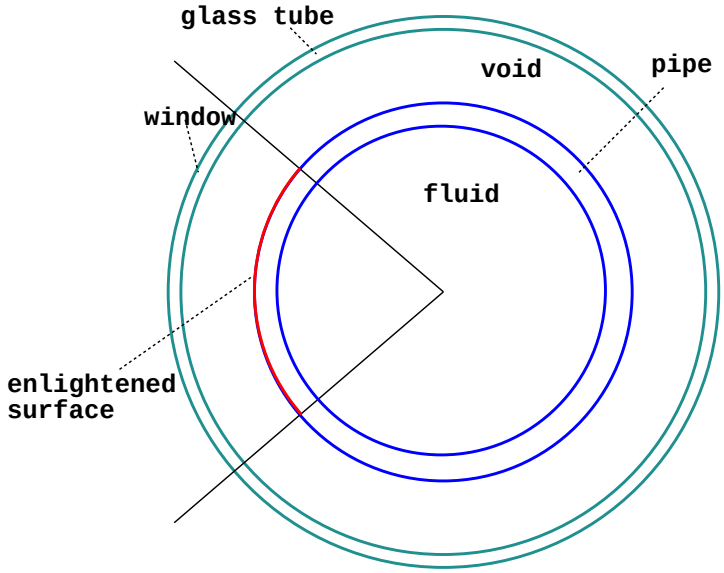

Figure 1: sketch of the solar tube.

Special coatings are used on solid surfaces in order to maximise the absorbed solar radiation and minimise thermal radiation losses to the environment. In particular, the enlightened pipe surface is treated with a spectrally selective coating with high absorptance at visible frequencies and low emittance at infrared frequencies.

3 The one-dimensional multi-zone model

3.1 Model description

The solar tube is discretised into n cells. Each cell is split into five zones, as illustrated in Figure 2, each of them being considered a control volume in thermal equilibrium. Sections at i and i+1 are the inlet and outlet sections of the fluid control volume (f), where the fluid variables (velocity, temperature, density, pressure and physical properties) are defined.

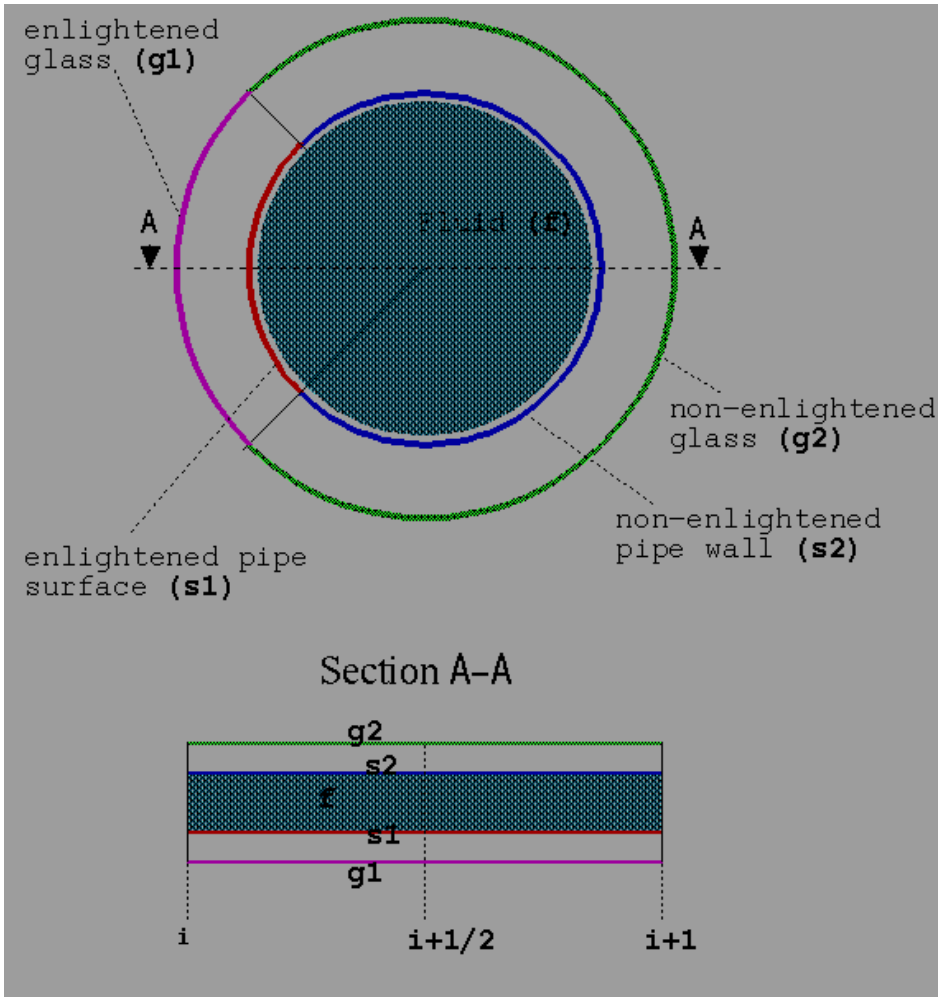

Figure 2: sketch of the topology of a 1D cell. Positions i and i+1 correspond to the inlet and outlet sections (where fluid variables are calculated). Solids variables and all heat exchange coefficients are calculated in the i+1/2 position.

Symbols	**Description**
Subscript **i**	fluid parameters at the inlet/outlet section
Subscript **f**	fluid parameters at the i+1/2 position
Subscripts **s1,s2**	Values on the two parts of the pipe surface
Subscripts **g1,g2**	Values on the two parts of the glass surface
Subscript **a**	External air
$\bar{R}_t$	Solar radiation incoming on the pipe surface (s1). [W/m^2]
Q_{sun}	Solar radiation absorbed by the enlightened part of the pipe (s1). [W]
Q	Convective heat exchanged (positive when absorbed) by the considered zone (f, s1, s2, g1, g2). [W]
Q_R	Net thermal radiation (positive when absorbed) exchanged by the considered zone (f, s1, s2, g1, g2). [W]
E, G, J	Surface thermal emissive power, incoming radiation and radiosity. [W]
H, h	Fluid total and thermal enthalpy. [J/kg]
T, v, p, p_t, C_p, ν, k	Fluid temperature [K], velocity [m/s], pressure [Pa], total pressure {Pa], specific heat at constant pressure [J/Kg/K], cinematic viscosity [m^2/s] and thermal conductivity [W/m/K].
ρ	Fluid density [Kg/m^3] (if referred to the fluid) or surface reflectance (if referred to a solid surface).
$(\Delta p_t)_d$	Total pressure loss due to friction. [Pa]
h	Convective heat exchange coefficient. [W/m^2/K]
β	Thermal expansion coefficient. [1/K]
g	Gravity acceleration. [m/s^2]
Re, Nu, Pr, Gr	Reynolds, Nusselt, Prandtl and Grashov numbers
ε_v, ρ_v, τ_v	Emittance, reflectance and transmittance at visible frequencies.
ε, ρ, τ	Emittance, reflectance and transmittance at infrared frequencies.
L	Cell length. [m]
D_i, D_e	Internal and external diameters of solid parts. [m]
A_i, A_e	Internal and external area of solid parts. [m^2]
m	Mass flow-rate. [Kg/s]
r	Pipe relative roughness.
f_f	Friction factor.

Table 1: list of symbols

Solid structures (namely the steel and glass pipes) are divided into two regions: the enlightened part (s1, g1) and the non-enlightened part (s2, g2). All the parameters of the solid parts are defined in the cell centres (position i+1/2), as well as all energy exchange and their coefficients. For a description of the symbols used see Table 1.

Fluid parameters in the cell centres are calculated as

$$\varphi_f = \varphi_{i+1/2} = \frac{(\varphi_{i+1} + \varphi_i)}{2} \tag{1}$$

where φ is any fluid parameter. The fluid (air) flow is governed by the following equations (subscripts have been omitted):

First equation of state: $$p = \rho R T \tag{2}$$

Second equation of state: $$h(T) = \int_0^T C_p(T)\, dT \; ; \quad h_{i+1} - h_i = \int_{T_i}^{T_{i+1}} C_p(T)\, dT \cong C_{p,f}(T_{i+1} - T_i) \tag{3}$$

Definition of total enthalpy: $$H = h + \frac{v^2}{2} \tag{4}$$

Definition of total pressure: $$p_t = p + \frac{1}{2}\rho v^2 \tag{5}$$

Total pressure losses due to friction: $$(\Delta p_t)_d = f_f \frac{L}{D_{i,s}} \rho \frac{v^2}{2} \tag{6}$$

where the friction factor f_f is given by [4]

$$f_f = 4 \left\{ 4 \log_{10} \left[0.27\, r + \left(\frac{7}{Re} \right)^{0.9} \right] \right\}^{-1}$$

Given the mass flow rate m and the inlet temperature T_i and pressure p_i, all fluid parameters at section i+1 can be deduced through the above equations. The relations used for the air physical properties are reported in Sec. 4.2.1.

Figure 3 shows the scheme of the energy exchange between the various parts of the cell. The following simplifications are considered:

- the solar radiation is transmitted and reflected by the glass window (no solar radiation is absorbed by the glass);
- the solar radiation reflected by the pipe surface does not participate to the energy balance;
- thermal radiation exchanges take place between s1 and g1 and between s2 and g2 separately. This means that all the radiation emitted from s1 (s2) is received from g1 (g2) and vice versa.

The following energy balances can be made for each zone of the cell.

Fluid (f)

The fluid (f) exchanges the convection heat Q_f with the two parts of the pipe (s1, s2), resulting in an increase of total enthalpy given by

$$\begin{aligned} Q_f &= m\,(H_{i+1} - H_i) = m\,[(h_{i+1} - h_i) + 0.5\,(v_{i+1}^2 - v_i^2)] = m\,[C_{p,i+1/2}(T_{i+1} - T_i) + 0.5\,(v_{i+1}^2 - v_i^2)] = \\ &= 2mC_{p,f}T_f + 0.5\,m\,(v_{i+1}^2 - v_i^2) \end{aligned} \tag{7}$$

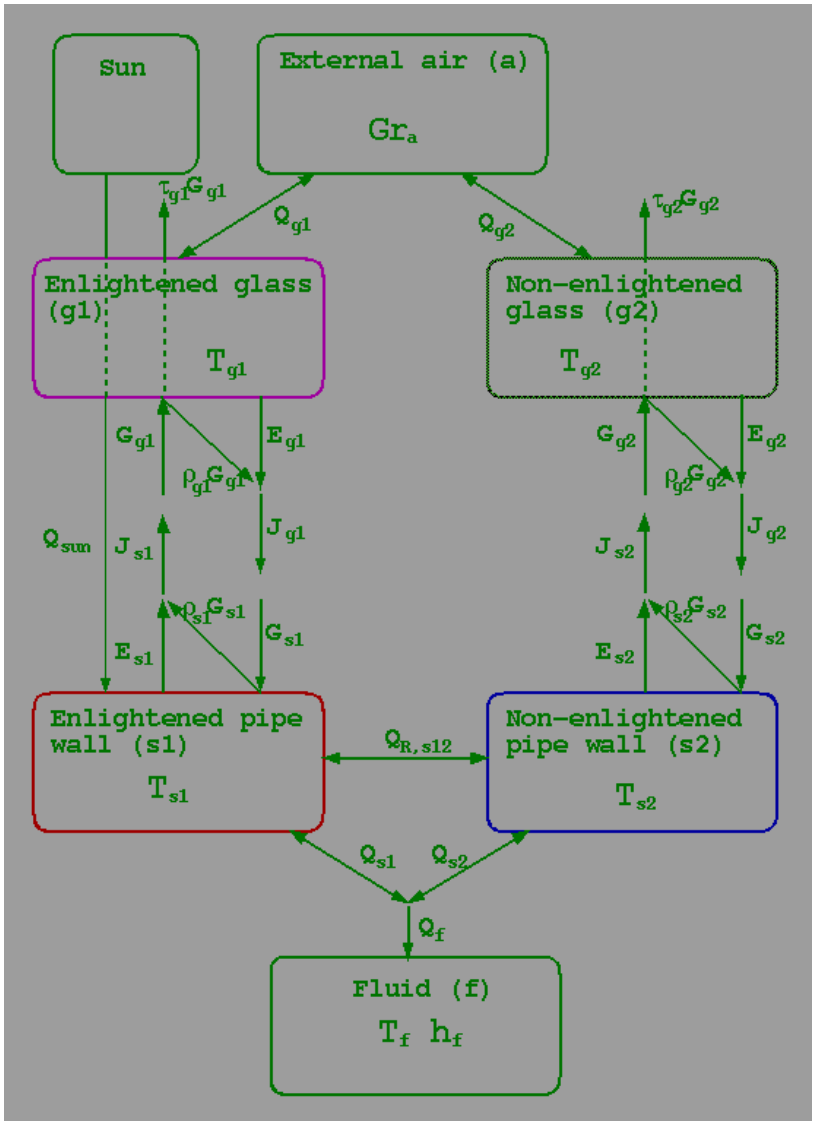

Figure 3: scheme of the energy exchange between the parts of the cell. The variables involved are reported inside each block.

Enlightened pipe (s1)

The enlightened part of the steel pipe (s1) absorbs the solar radiation

$$Q_{sun} = \varepsilon_{v,s1} A_{e,s1} \bar{R}_t \tag{8}$$

being $\bar{R}_t$ the concentrated solar radiation incoming on the pipe surface, exchanges the convection heat

$$Q_{s1} = A_{i,s1} h_f (T_f - T_{s1}) \tag{9}$$

with the fluid (f), and the radiation $Q_{R,s1}$ with the enlightened part of the glass pipe (g1) (the expression for $Q_{R,s1}$ is given further on).

Non-enlightened pipe (s2)

The non-enlightened part of the steel pipe (s2) exchanges the convection heat

$$Q_{s2} = A_{i,s2}\, h_f\, (T_f - T_{s2}) \tag{10}$$

with the fluid (f), and the radiation $Q_{R,s2}$ with the non-enlightened part of the glass pipe (g2). The heat exchange coefficient h_f is given by [4]

$$h_f(T_f) = \frac{Nu_f k_f}{D_{i,s}} \qquad \text{where} \qquad Nu_f = 0.023\, Re_f^{0.8}\, Pr_f^{0.4} \tag{11}$$

Enlightened glass (g1)

The enlightened part of the glass pipe (g1) exchanges the natural convection heat

$$Q_{g1} = A_{e,g1}\, h_{a,g1}(T_a - T_{g1}) \tag{12}$$

with the external air (a), and the radiation $Q_{R,g1}$ with the enlightened part of the steel pipe (s1). In this case part of the radiation incoming on g1 is transmitted outside the control volume (an expression for $Q_{R,g1}$ is given further on). The solar radiation absorbed by the glass is neglected in this model.

Non-enlightened glass (g2)

The non-enlightened part of the glass pipe (g2) exchanges the natural convection heat

$$Q_{g2} = A_{e,g2}\, h_{a,g2}\, (T_a - T_{g2}) \tag{13}$$

with the external air (a), and the radiation $Q_{R,g2}$ with the enlightened part of the steel pipe (s1).

The natural convection heat exchange between the glass tube and the external air has been modelled on the basis of empirical relations for natural convection around pipes. The expression for the heat exchange coefficients for g1 and g2 are given by [5]

$$h_{a,g} = \frac{Nu_a k_a}{D_{e,g}} \quad \text{where} \quad Nu_a = 0.604\, c\, Gr_a^{0.25} \quad \text{and} \quad Gr_a = \frac{g\, \beta_a\, D_{e,g}^3\, |T_g - T_a|}{\nu_a^2} \tag{14}$$

where c is, in general, a function of the angular position (see [5] and Sec. 4.4.4). In this case the mean values c =0.75 for g1 and c =0.5 for g2 were set.

The expressions for the contribution involved in the radiation exchange between s1-g1 and s2-g2 are listed in Table 2. Combining these expressions, the following relations for the radiation heat absorbed by s1, s2, g1 and g2 can be deduced:

$$\left[Q_{R,s} = \frac{\varepsilon_s}{1-\rho_g\rho_s} E_g - \frac{\varepsilon_g}{1-\rho_g\rho_s} E_s = \frac{\sigma\varepsilon_g\varepsilon_s A_{i,g}}{1-\rho_g\rho_s} T_g^4 - \frac{\sigma\varepsilon_s(1-\rho_g)A_{e,s}}{1-\rho_g\rho_s} T_s^4 \right]_{1,2} \tag{15}$$

$$\left[Q_{R,g} = \frac{\varepsilon_g}{1-\rho_g\rho_s} E_s - \frac{1-\rho_g\rho_s-\varepsilon_g\rho_s}{1-\rho_g\rho_s} E_g = \frac{\sigma\varepsilon_s\varepsilon_g A_{e,s}}{1-\rho_g\rho_s} T_s^4 - \frac{(1-\rho_g\rho_s-\varepsilon_g\rho_s)\sigma\varepsilon_g A_{i,g}}{1-\rho_g\rho_s} T_g^4 \right]_{1,2} \tag{16}$$

The radiation exchange between the two parts of the steel pipe ($Q_{R,s12}$) through the air flow is also taken into account in the form

$$Q_{R,s12} = c_{R,s12}\, (T_{s2}^4 - T_{s1}^4)$$

where $c_{R,s12}$ is a factor which depends on the view factors between s1 and s2, so depending on the pipe internal diameter. In this modelling, as a first approximation, it has been considered constant and its average value calculated through the 3D CFD model for different diameters, yielding

$$c_{R,s12} \cong 1.4 \infty 10^{-9}$$

The heat $Q_{R,s12}$ is added to $Q_{R,s1}$ and subtracted from $Q_{R,s2}$.

	E [W]	**G** [W]	**J** [W]	$\mathbf{Q_R}$ [W]
s1	$A_{e,s1}\ \varepsilon_{s1}\ \sigma\ T_{s1}^4$	J_{g1}	$E_{s1} + \rho_{s1}\ G_{s1}$	$G_{s1} - J_{s1}$
s2	$A_{e,s2}\ \varepsilon_{s2}\ \sigma\ T_{s2}^4$	J_{g2}	$E_{s2} + \rho_{s2}\ G_{s2}$	$G_{s2} - J_{s2}$
g1	$A_{i,g1}\ \varepsilon_{s1}\ \sigma\ T_{g1}^4$	J_{s1}	$E_{g1} + \rho_{g1}\ G_{g1}$	$G_{g1} - J_{g1} - \tau_{g1}\ G_{g1}$
g2	$A_{i,g2}\ \varepsilon_{g2}\ \sigma\ T_{g2}^4$	J_{s2}	$E_{g2} + \rho_{g2}\ G_{g2}$	$G_{g2} - J_{g2} - \tau_{g2}\ G_{g2}$

Table 2: thermal radiation balance.

Making the energy balance of all the parts of the control volume yields the following system of 5 equations:

$$\begin{cases} Q_f + Q_{s1} + Q_{s2} = 0 \\ Q_{sun} + Q_{R,s1} + Q_{s1} = 0 \\ Q_{R,s2} + Q_{s2} = 0 \\ Q_{g1} + Q_{R,g1} = 0 \\ Q_{g2} + Q_{R,g2} = 0 \end{cases} \tag{17}$$

in the 5 unknowns T_f, T_{s1}, T_{s2}, T_{g1}, T_{g2}.

The mathematical model described above has been implemented in the EXCEL framework and solved iteratively.

3.2 Model limitations

The main limitations of the model described above (apart from the intrinsic limitations of a 1D model) are the following:

the solar radiation absorbed by the glass window is not considered, as well as the solar radiation reflected by the pipe surface.

All the radiation leaving s1 (s2) is supposed to be received by g1 (g2) and vice-versa, while actually there is a radiation exchange between s1 and g2 and between s2 and g1.

The heat transferred from s1 to s2 by thermal conduction is not taken into account (it could be not negligible, especially if a copper layer is used to enhance this effect). Thermal conduction along the axis is not considered as well (it has, however, a minor effect).

Thermal radiation from the glass tube external surface to the environment is not modelled.

Thermal radiation inside the pipe is modelled through a constant coefficient which was evaluated from the 3D model and which actually varies with the pipe diameter.

4 The three-dimensional CFD model

4.1 Description

CFD calculations were performed using Star-CD. Both fluids and solids were simulated in coupled way, taking into account both conduction inside solids and radiation among solid surfaces. The geometry and the mixed structured-unstructured computational mesh were built with the IDEAS CAD/mesh generator. The model is fully parametric.

Figure 4 shows the topology of the CFD model together with the computational mesh. The pipe is made of two adjacent layers of different materials, in order to be able to simulate the insertion of an inner pipe of more conductive material with the scope of enhancing the thermal conduction in the tangential direction. In all the simulations reported in this work, a pipe made of a layer of steel and a layer of copper was considered.

The pipe is insulated by an external glass pipe; void is made in the space between the glass tube and the metal tube.

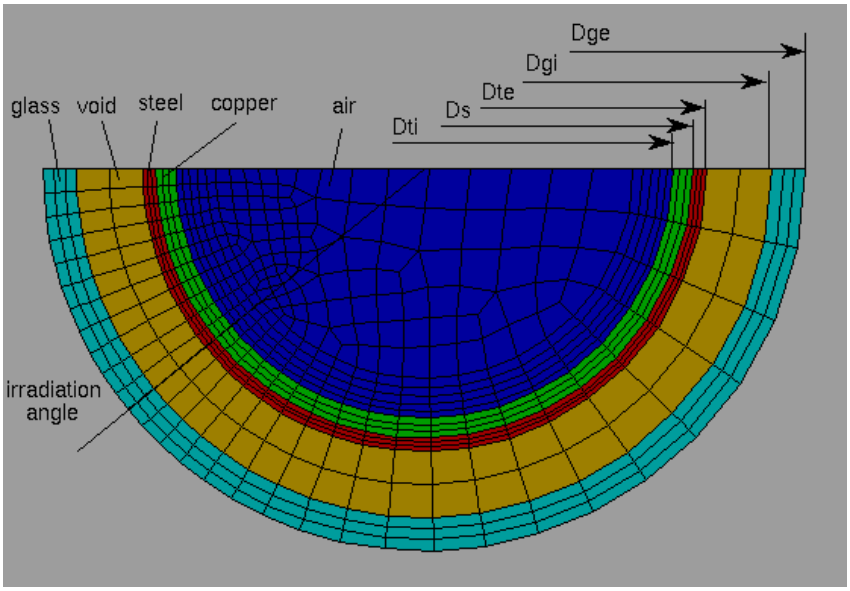

Figure 4: topology of the CFD model and computational mesh.

4.2 Physical modelling

The collector irradiation is simulated with an imposed heat flux in the enlightened part of the tube external wall. Thermal radiation is calculated both inside the pipe and from the external pipe surface to the glass-pipe surface, which was considered an absorbing-reflecting-transmitting surface. Both the air and the void region were considered as transparent media. The fraction of solar radiation reflected by the enlightened surface was not simulated.

The thermal field of the glass tube was simulated considering the thermal-radiation exchanges with the steel pipe and the cooling by the ambient air. This last effect was modelled on the basis of empirical relations for natural convection around pipes, as described in Sec. 4.4.4. The absorption of solar radiation and the thermal radiation to the environment were not taken into account.

The void was simulated as a laminar flow with negligible thermal conductivity (10^{-6} W/m/K). If required, the simulation of the low-density air can be performed with accuracy (for example to study the effect of different pressure conditions).

The physical properties of the considered materials are listed below (based on data extracted form [5]):

4.2.1 Air properties

Density: ideal gas

Viscosity (Kg/m/s): Sutherland's Law

≠ $\mu = \mu_0 \left(\frac{T}{T_0} \right)^{1.5} \frac{c_s + T_0}{c_s + T}$ (T in K)

≠ $\mu_0 = 1.716 \cdot 10^{-5}$, $T_0 = 273$ K, $c_s = 116$

≠ μ (773 K) = 3.594×10^{-5} Kg/m/s

Thermal conductivity (W/m/K): polynomial

≠ $k = -6.8796 \cdot 10^{-12} T^3 + 5.2695 \cdot 10^{-9} T^2 + 5.8941 \cdot 10^{-5} T + 7.998 \cdot 10^{-3}$ (T in K)

≠ Validity range: 255 K - 1644 K

≠ k (773 K) = 5.353×10^{-2} W/m/K

Specific heat (J/Kg/K): polynomial

≠ $C_p = -1.2356 \cdot 10^{-7} T^3 + 3.2198 \cdot 10^{-4} T^2 - 5.8442 \cdot 10^{-7} T + 995.5281$ (T in K)

≠ Validity range: 255 K - 1644 K

≠ C_p (773 K) = 1085.7 J/Kg/K

4.2.2 Steel properties

Density: $\rho = 7800$ Kg/m^3

Thermal conductivity: k = 24 W/m/K

Specific heat: C = 460 J/Kg/K

4.2.3 Copper properties

Density: $\rho = 8900$ Kg/m^3

Thermal conductivity: k = 350 W/m/K

Specific heat: C = 380 J/Kg/K

4.3 Computational mesh

A mixed structured-unstructured mesh was used (see Figure 4). Structured meshes were used for the near-wall fluid region, for solid layers and for the void region. 100 cells were used in the axial direction, for a total number of cells of about 60000.

4.4 Boundary conditions

4.4.1 Inlet / outlet

Inlet: imposed constant velocity and temperature;

Outlet: extrapolation with mass flow rate conservation condition;

4.4.2 Collector irradiation

In the models described in [6] and [7], the collector irradiation was simulated as a heat flux on the pipe enlightened surface. In the case where the glass pipe is simulated, it is not possible to apply the same condition in StarCD, being the enlightened surface an interface between two media. Therefore, the concentrated solar irradiation was simulated through a volumetric heat source applied to the first layer of cells near the enlightened surface. The heat source (W/m^3) was calculated as

$$\dot{q} = \frac{Q_{sun}}{V_{irr}}$$

where Q_{sun} is the total solar radiation absorbed by the enlightened part of the pipe (Eq. 14) and V_{irr} is the total volume of the first layer of cells next to the enlightened surface.

4.4.3 Internal walls

All internal surfaces are interfaces between different media and are treated as radiating-conducting walls with zero interface resistance. All radiating walls are treated as grey opaque surfaces apart from the glass surface, which is treated as an emitting-reflecting-transmitting surface.

4.4.4 Glass tube external surface

The glass tube external surface was considered a constant-temperature wall with a heat resistance given by

$$r = 1/h_c$$

where the empirical correlation for natural convection cooling of a cylinder (see also Eq. 20) was used for the thermal conductivity, namely

$$h_c = 0.604\, c(\alpha)\, Gr^{0.25} \qquad (18)$$

where

$$Gr = \frac{g\beta_0(T_w - T_0)D_{ge}^3}{\nu_0^2}$$

$T_0 = 293$ K, $\beta_0 = 1/T_0 = 3.4\ 10^{-3}$ 1/K, $\nu_0 = 1.5\ 10^{-5}$ m^2/s

being all properties referred to air at 20 °C. In this case the coefficient in Eq. 24 is a function of the angular position, namely

$$c(\alpha) = 6.38 \cdot 10^{-8}\ \alpha^3\ -\ 3.60 \cdot 10^{-5}\ \alpha^2\ +\ 7.17 \cdot 10^{-3}\ \alpha\ +\ 0.266$$

where the angle α is calculated starting from the point opposite to the collector window, having considered the window oriented towards the ground.

For practical reasons, the temperature of the first cell beside the boundary was used as T_w.

4.5 Model limitations

The main limitations of the model described above are the following:

solar irradiation is modelled as a constant source term, while in the reality it is a function of the position.

The solar radiation absorbed by the glass window is not considered, as well as the solar radiation reflected by the pipe surface.

The thermal radiation from the glass tube external surface to the environment is not modelled.

All radiating properties are constant.

All the above limitations can be removed with a model development.

4.6 Numerical set-up

4.6.1 Type of simulation

Turbulent flow with fluid-solid conjugate heat transfer and thermal radiation. All media are considered transparent.

4.6.2 Integration algorithm and parameters

The SIMPLE algorithm was used for all the calculations. Some convergence problems arose in the simulation of the 100 m tube, solved increasing the number of sweeps (2000) and reducing the residual tolerance (0.001) of the pressure equation. Using double-precision compilation was also necessary.

4.6.3 Turbulence modelling

Chen k-ε model with Wall-Functions.

4.6.4 Convective schemes

Momentum equations: QUICK.

Energy equation: QUICK

Turbulence equations: UPWIND

Density: Central Difference

4.7 Computational times

For a given topology, the test case set-up, included the mesh generation from IDEAS and the final check-up, takes about 30 min. The computational time on one node of the IBM SP3 (serial calculation) is order 4 hours.

5 System efficiency

With reference to the scheme shown in Figure 5, the solar collector system global efficiency can be defined as

$$\eta_g = \frac{Q_o - Q_p}{R_{s,c}} = \frac{Q_i}{R_{s,c}} \frac{Q_o - Q_p}{Q_i} = \eta_R \eta_p \tag{19}$$

where

≠ $R_{s,c}$ solar radiation power concentrated form the parabola onto the pipe surface [W];

≠ Q_i thermal power absorbed by the fluid;

≠ Q_o thermal power transferred from the heat exchanger to the downstream systems;

≠ $\eta_R = \frac{Q_i}{R_{s,c}}$ radiation collection efficiency;

≠ $\eta_p = \frac{Q_o - Q_p}{Q_i}$ pumping efficiency.

Q_p is the fraction of Q_o converted into electrical power and used to pump the fluid, namely

$$Q_p = \frac{W_p}{\eta_{el}}$$

where W_p is the pumping power and $\eta_{el} = \frac{W_{el}}{Q_o}$ is the electrical overall efficiency of the system downstream the solar collector system.

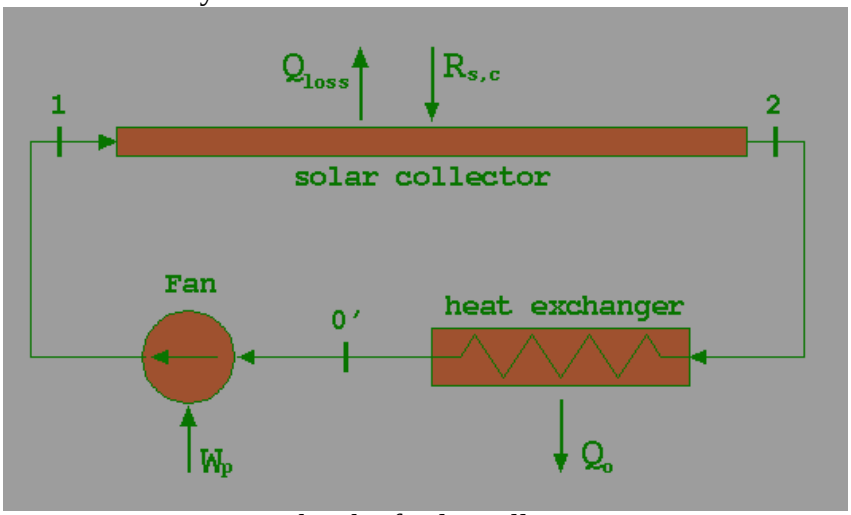

Figure 5: sketch of solar collector system

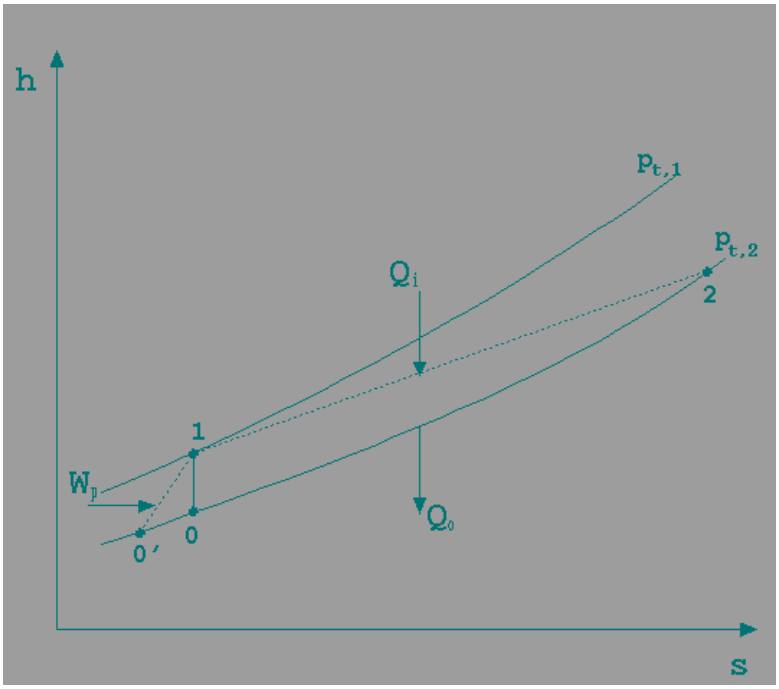

Figure 6: sketch of the thermodynamic cycle of the solar collector.

Lacking other information, we assume negligible pressure losses in the heat exchanger. In these conditions, the thermal cycle of the solar collector can be described as in Figure 6. The following relations can be written

$$Q_o = Q_i + W_p$$

$$Q_i = R_{s,c} - Q_{loss} = R_{s,c} - |Q_{R,s1} + Q_{R,s2}|$$

$$W_p = \frac{1}{\eta_c} W_{p,is}$$

where η_c is the fan efficiency, and $W_{p,is}$ is the isentropic compression power necessary to rise the fluid pressure from $p_{t,1}$ to $p_{t,2}$, given by

$$W_{p,is} = m(H_1 - H_0) = m\int_0^1 \frac{dp_t}{\rho} = m\frac{\gamma}{\gamma-1}\frac{p_{t,0}}{\rho_0}\left[\left(\frac{p_{t,1}}{p_{t,0}}\right)^{\frac{\gamma}{\gamma-1}} - 1\right] = m\frac{\gamma}{\gamma-1}\frac{p_{t,2}}{\rho_1}\left(\frac{p_{t,1}}{p_{t,2}}\right)^{\frac{1}{\gamma}}\left[\left(\frac{p_{t,1}}{p_{t,2}}\right)^{\frac{\gamma}{\gamma-1}} - 1\right]$$

Finally, we can write

$$\eta_R = 1 - \frac{Q_{loss}}{R_{s,c}} = 1 - \frac{|\,Q_{R,s1} + Q_{R,s2}\,|}{R_{s,c}} \qquad (20)$$

$$\eta_p = 1 - \frac{(1/\eta_{el} - 1)\,W_p}{Q_i} \qquad (21)$$

6 Comparison between the 1D model and the 3D-CFD model results

A set of calculations was performed in order to optimise the pipe internal diameter and to validate the 1D model against the CFD model. The fixed parameters are listed in Table 3, Table 4 and Table 5. It should be noted that the radiating properties at visible frequencies were used only to determine the portion of solar radiation absorbed by the enlightened part of the pipe. No radiation calculations were performed at visible frequencies.

Parameter	**Symbol**	**Value**
Tube length	L_t	100 m
Steel layer thickness	s_s	2 mm
Copper layer thickness	s_c	3 mm
Void gap thickness	s_v	10 mm
Glass thickness	s_g	5 mm
Angle of irradiation	$\Delta\varphi$	72 deg
Collected solar radiation	$R_{s,c}$	600 kW
Inlet temperature	T_{in}	350 °C
Inlet pressure	p	20 bar
Pipe internal roughness	r	0

Table 3: global (fixed) parameters.

Surface	**Absorptance (α_v)**	**Reflectance (ρ_v)**	**Transmittance (τ_v)**
Glass surface	0	0.03	0.97
Enlightened steel	1	0	-

Table 4: radiating properties of enlightened surfaces at visible frequencies

Surface	**Emittance (ε)**	**Reflectance (ρ)**	**Transmittance (τ)**
Copper-air surface	0.77	0.23	-
Enlightened steel-void surface	0.19	0.81	-
Non-enlightened steel-void surface	0.01	0.99	-
Glass-void surface	0.9	0	0.1

Table 5: radiating properties of internal surfaces at infrared.

Four diameters where considered (75, 100, 120 and 140 mm). In all cases mass flow rates were automatically tuned in order to get an outlet air temperature of 600 °C.

6.1 Internal pipe diameter $D_{i,s}$ = 75 mm

Table 6 shows the air parameters at the outlet section. Being the outlet temperature imposed, the parameters relevant for the comparison of the two models are the mass flow rate and the total pressure loss. In this case the agreement between the two models is quite good. This is confirmed by Table 7, where the heat balances and the efficiencies are reported. The 1D model overestimates radiation losses transmitted across the glass tube (8 %) and slightly underestimates radiation losses removed from external air (1.4 %), resulting in an error of 4.1 % on the total radiation loss and of 0.2 % in the estimation of the radiation collection efficiency. In this case the main error can be found in the evaluation of the pumping efficiency (1.2 %), which is also the main responsible for the low global efficiency (0.81). The error on the global system efficiency is 1.4 %.

Quantity	**3D model**	**1D model**	**Difference**
Mass flow rate	2.039 Kg/s	2.032 Kg/s	0.3 %
Outlet temperature	600.1 °C	600.1 °C	0.0 %
Outlet density	7.22 Kg/m^3	7.21 Kg/m^3	0.1 %
Outlet velocity	64.09 m/s	63.77 m/s	0.5 %
Total pressure loss	185055 Pa	186039 Pa	0.5 %

Table 6: flow mean values at the outlet section for $D_{i,s}$ = 75 mm.

Power balances	**Symbol**	**3D model**	**1D model**	**Difference**
Net thermal radiation from the pipe surface = total heat loss	$R_{pe}=Q_{loss}$ (R_{pe} / Q_{sun})	29.2 kW (5.0 %)	30.4 kW (5.2 %)	4.1 %
Total thermal radiation transmitted across the glass	$R_{g,\tau}$ ($R_{g,\tau}$ / Q_{sun})	7.5 kW (1.3 %)	9.0 kW (1.5 %)	8 %
Net thermal radiation absorbed by the glass = heat removed from external air cooling	Q_{ext} (Q_g / Q_{sun})	21.7 kW (3.7 %)	21.4 kW (3.7 %)	1.4 %
Radiation collection efficiency	η_R	0.921	0.919	0.2 %
Pumping power (η_c = 0.8)	W_p	43.4 kW	47.4 kW	9.2 %
Pumping efficiency (η_{el} = 0.4)	η_p	0.882	0.871	1.2 %
System efficiency	η_g	0.812	0.801	1.4 %

Table 7: global energy balance and efficiency for $D_{i,s}$ = 75 mm (absorbed solar radiation Q_{sun} = 582 kW).

6.2 Internal pipe diameter $D_{i,s}$ = 100 mm

Increasing the diameter has the effect of increasing the error on the calculation of the radiation efficiency (0.6 %). However, in this case, the error on the evaluation of the pumping efficiency is much lower (0.3 %), yielding an error on the global efficiency of 1 %.

The system efficiency is considerably higher with respect to the previous one (0.88) due to a better balance of radiation and pumping losses.

Quantity	**3D model**	**1D model**	**Difference**
Mass flow rate	2.011 Kg/s	1.993 Kg/s	0.9 %
Outlet temperature	600.2 °C	600.2 °C	0.0 %
Outlet density	7.80 Kg/m^3	7.80 Kg/m^3	0 %
Outlet velocity	32.91 m/s	32.54 m/s	1.1 %
Total pressure loss	43154 Pa	43121 Pa	0.1 %

Table 8: flow mean values at the outlet section for $D_{i,s}$ = 100 mm.

Power balances	**Symbol**	**3D model**	**1D model**	**Difference**
Net thermal radiation from the pipe surface = total heat loss	$R_{pe}=Q_{loss}$ (R_{pe} / Q_{sun})	39.0 kW (6.7 %)	42.7 kW (7.3 %)	9.5 %
Total thermal radiation transmitted across the glass	$R_{g,\tau}$ ($R_{g,\tau}$ / Q_{sun})	10.5 kW (1.8 %)	13.4 kW (2.3 %)	27.6 %
Net thermal radiation absorbed by the glass = heat removed from external air cooling	Q_{ext} (Q_g / Q_{sun})	28.6 kW (4.9 %)	29.3 kW (5.0 %)	2.4 %
Radiation collection efficiency	η_R	0.905	0.899	0.6 %
Pumping power (η_c = 0.8)	W_p	9.8 kW	10.6 kW	8.2 %
Pumping efficiency (η_{el} = 0.4)	η_p	0.973	0.970	0.3 %
System efficiency	η_g	0.881	0.872	1 %

Table 9: global energy balance and efficiency for $D_{i,s}$ = 100 mm (absorbed solar radiation Q_{sun} = 582 kW).

6.3 Internal pipe diameter $D_{i,s}$ = 120 mm

The same tendency can be observed in this case. The error on the global efficiency is 1.2 %, being the main responsible the error on the radiation efficiency (1.1 %).

The global efficiency is the same as the case with $D_{i,s}$ = 100 mm, implying that the optimum value of the internal diameter is in between these two values (see Sec. 6.5).

Quantity	**3D model**	**1D model**	**Difference**

Mass flow rate	1.980 Kg/s	1.953 Kg/s	1.4 %
Outlet temperature	600.4 °C	600.4 °C	0.0 %
Outlet density	7.91 Kg/m^3	7.91 Kg/m^3	0.0 %
Outlet velocity	22.20 m/s	21.85 m/s	1.6 %
Total pressure loss	17303 Pa	17135 Pa	1.0 %

Table 10: flow mean values at the outlet section for $D_{i,s}$ = 120 mm.

Power balances	**Symbol**	**3D model**	**1D model**	**Difference**
Net thermal radiation from the pipe surface = total heat loss	$R_{pe}=Q_{loss}$ (R_{pe} / Q_{sun})	47.4 kW (8.1 %)	53.4 kW (9.2 %)	12.7 %
Total thermal radiation transmitted across the glass	$R_{g,\tau}$ ($R_{g,\tau}$ / Q_{sun})	13.2 kW (2.3 %)	17.5 kW (3.0 %)	32.6 %
Net thermal radiation absorbed by the glass = heat removed from external air cooling	Q_{ext} (Q_g / Q_{sun})	34.2 kW (5.9 %)	35.9 kW (6.2 %)	5.0 %
Radiation collection efficiency	η_R	0.891	0.881	1.1 %
Pumping power (η_c = 0.8)	W_p	3.8 kW	4.2 kW	10.5 %
Pumping efficiency (η_{el} = 0.4)	η_p	0.989	0.988	0.1 %
System efficiency	η_g	0.881	0.870	1.2 %

Table 11: global energy balance and efficiency for $D_{i,s}$ = 120 mm (absorbed solar radiation Q_{sun} = 582 kW).

A more extensive comparison between the 1D and 3D models is presented in this case. Figure 7 shows the mean-temperature distributions in the fluid and in the two parts of the pipe (s1 and s2) along the pipe. The 1D model overestimates the temperature in the enlightened part of the pipe while underestimates the pipe temperature in the rest of the pipe (a possible explanation to this behaviour is discussed in Sec. 6.6). These two errors partially compensate each other, resulting a good estimation of thermal losses, as can be seen in Figure 8. Here the cumulative radiation losses as a percentage of the total losses and the local radiation losses as a percentage of the absorbed solar radiation are drawn as a function of the position along the pipe.

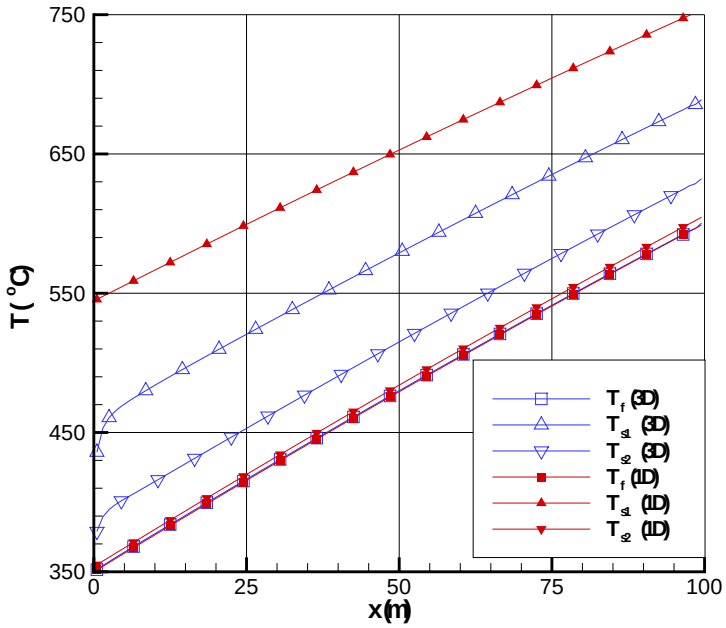

Figure 7: comparison between the 3D and 1D models of the distribution of the mean temperatures in the enlightened (s1) and non-enlightened (s2) parts of the pipe wall.

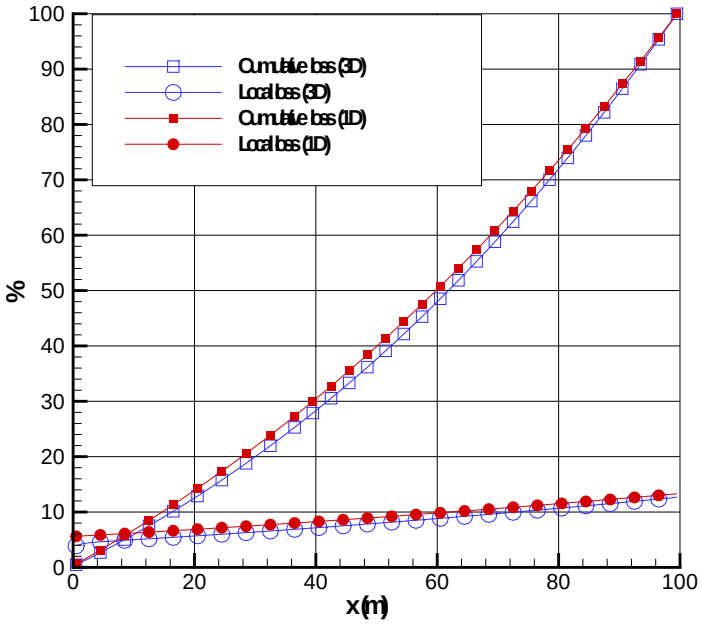

Figure 8: comparison between the 3D and 1D models of the distribution of cumulative (as a percentage of the total loss) and local (as a percentage of absorbed solar radiation) radiation losses along the pipe.

It can be noticed that the non-linearity of these curves is not so marked. This is due to the fact that only the thermal radiation transmitted across the glass (which is 10 % of the thermal radiation from the pipe surface) is a function of the fourth power of temperature, being the rest removed from external air convection.

Figure 9 shows the temperature fields in the fluid and in the pipe (on the left) and in the glass tube (on the right). The maximum temperature is obviously found in the steel layer of the pipe (700 °C).

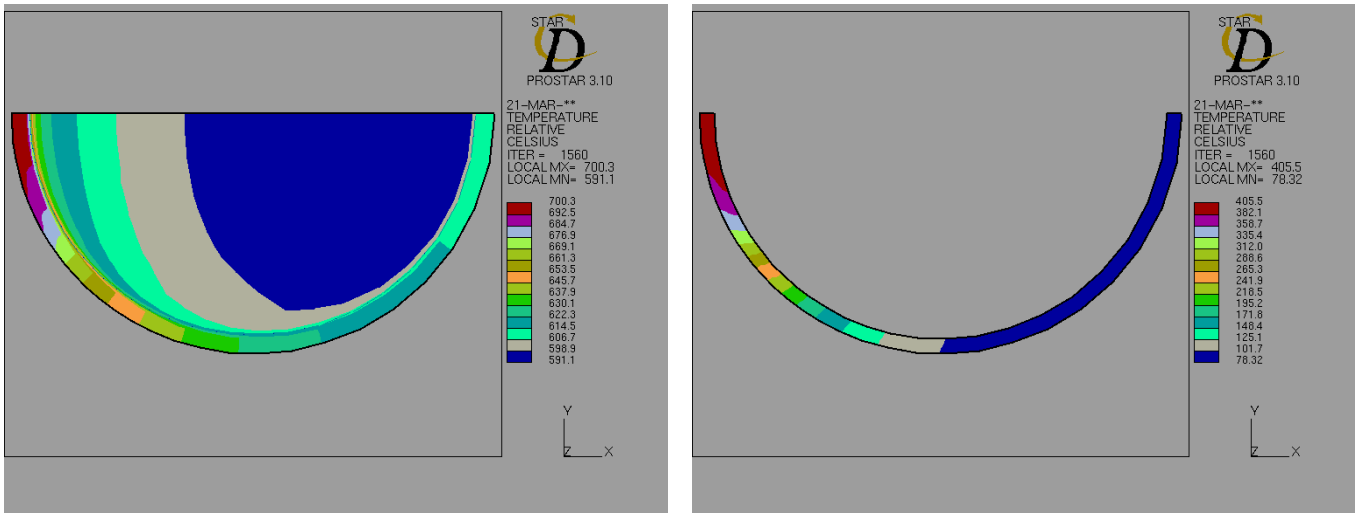

Figure 9: outlet section temperature fields inside the fluid and the pipe (on the left) and inside the glass tube (on the right).

6.4 Internal pipe diameter $D_{i,s}$ = 140 mm

In this case the decrease of the radiation collection efficiency (0.88) is no more compensated by the increase of the pumping efficiency (0.99), resulting in a worsening of the global efficiency (0.87).

The error on the evaluation of the radiation efficiency is the highest (1.7 %), as well as the error on the global efficiency (1.8 %)

Quantity	**3D model**	**1D model**	**Difference**
Mass flow rate	1.957 Kg/s	1.919 Kg/s	1.9 %
Outlet temperature	599.5 °C	599.5 °C	0.0 %
Outlet density	7.95 Kg/m^3	7.95 Kg/m^3	0.0 %
Outlet velocity	16.03 m/s	15.69 m/s	2.1 %
Total pressure loss	8034 Pa	7873 Pa	2.0 %

Table 12: flow mean values at the outlet section for $D_{i,s}$ = 140 mm.

Power balances	**Symbol**	**3D model**	**1D model**	**Difference**
Net thermal radiation from the pipe surface = total heat loss	$R_{pe}=Q_{loss}$ (R_{pe} / Q_{sun})	55.9 kW (9.6 %)	64.6 kW (11.1 %)	15.5 %
Total thermal radiation transmitted across the glass	$R_{g,\tau}$ ($R_{g,\tau}$ / Q_{sun})	16.1 kW (2.8 %)	22.0 kW (3.8 %)	36.6 %
Net thermal radiation absorbed by the glass = heat removed from external air cooling	Q_{ext} (Q_g / Q_{sun})	39.9 kW (6.9 %)	42.6 kW (7.3 %)	6.8 %
Radiation collection efficiency	η_R	0.877	0.862	1.7 %
Pumping power (η_c = 0.8)	W_p	1.76 kW	1.9 kW	10.5 %
Pumping efficiency (η_{el} = 0.4)	η_p	0.995	0.995	0.0 %
System efficiency	η_g	0.873	0.857	1.8 %

Table 13: global energy balance and efficiency for $D_{i,s}$ = 140 mm (absorbed solar radiation Q_{sun} = 582 kW).

6.5 Efficiency optimisation

Figure 10 shows the radiation, pumping and global efficiencies as a function of the pipe internal diameters for the two models. It can be deduced as, with this configuration, the optimum diameter is $D_{i,s}$ ♠ 110 mm. The same result is found both with the 1D and with the 3D models.

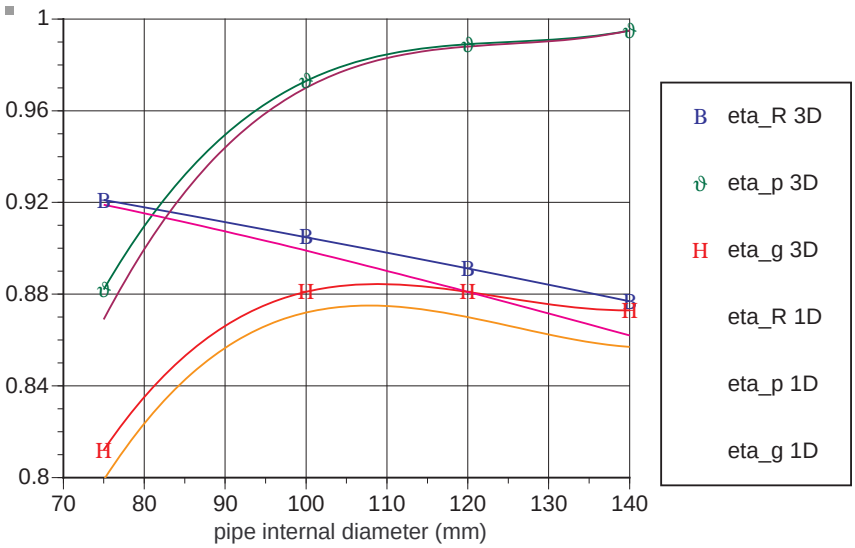

Figure 10: system efficiencies as a function of the pipe internal diameter for the 3D and the 1D models

6.6 Comments

The main reason for the discrepancy between the 1D and the 3D model is likely the presence in the 3D model of the copper layer, which strongly enhance the thermal conduction from the enlightened part of the pipe to the rest of the pipe. The 1D model does not take into account this effect., resulting in higher temperatures of the enlightened part of the pipe (s1). Furthermore, the actual view factors between the pipe and the glass tube are not calculated, having assumed no radiation exchange between s1 and g2 and between s2 and g1.

7 Conclusions

A one-dimensional multi-zone model and a 3D-CFD model have been developed for the analysis and optimisation of the solar collector pipe of the thermal solar plant proposed by C. Rubbia. Both models take into account the main physical phenomena involved in the problem.

The 1D model, implemented in a EXCEL framework, can be used to get instantaneous answers to parameters changes with an acceptable degree of accuracy.

The 3D-CFD model can give any information about local field variables and energy balances and can be used to confirm the 1D model estimations.

The results of the two models have been compared with a parametric study of the system efficiency as a function of the pipe internal diameter. Although differences up to 35 % were found in local radiation balances, the bigger difference in the global system efficiency was less than 2 %. The result of the optimisation was the same for both models, yielding an optimal pipe internal diameter of 110 mm.

8 References

[1] C. Rubbia, "Geometry of parabolic collectors for solar thermal energy production", ENEA/TM/PRES/2001_02, January 2001

[2] C. Rubbia, "High temperature parabolic collectors for solar thermal energy production", ENEA/TM/PRES/2001_03, January 2001

[4] Perry, Don Green, Perry's chemical engineers' handbook, Mc Graw Hill, 1997

[5] F. Kreith, "Principi di trasmissione del calore", Liguori Editore, 1988

[6] L. Maciocco, "Simulation of an air flow in a circular pipe irradiated by a linear parabolic solar collector (tube internal diameter Di = 120 mm)", February 2001, CRS4/EA/Internal Note 01-01

[7] L. Maciocco, "Simulation of an air flow in a circular pipe irradiated by a linear parabolic solar collector (tube internal diameter Di = 75 mm): effect of thermal radiation", February 2001, CRS4/EA/Internal Note 01-02

[8] L. Maciocco, " Simulation of an air flow in a circular pipe irradiated by a linear parabolic solar collector (tube internal diameter D_i = 75 mm, variable air properties, thermal radiation, external air cooling): effect of a reflecting film on the glass surface", February 2001, CRS4/EA/Internal Note 01-03

[9] L. Maciocco, " Simulation of an air flow in a circular pipe irradiated by a linear parabolic solar collector (tube internal diameter D_i = 75 mm, variable air properties, thermal radiation, external air cooling): effect of a dichroic film on the steel surface.", February 2001, CRS4/EA/Internal Note 01-04

[10] L. Maciocco, "Simulation of an air flow in a circular pipe irradiated by a linear parabolic solar collector", February 2001, CRS4/EA/Internal Note 01-06

[11] http://www.adapco.com

[12] http://www.scdc.com/ideas/index.shtml